minerals

MDPI

Article

Sulfidation of Smithsonite via Microwave Roasting under Low-Temperature Conditions

Jiawei Kang [1], Shubiao Yin [1,*], Mingxiao Li [2,*], Xingzhi Zhang [1], Xujie Wen [3], Hanping Zhang [2], Qi Nie [2] and Ting Lei [1]

[1] School of Metallurgy and Energy Engineering, Kunming University of Science and Technology, Kunming 650093, China; kangjiawei@stu.kust.edu.cn (J.K.); zxz18712801190@gmail.com (X.Z.); leitingkmyz@163.com (T.L.)
[2] School of Metallurgy and Mines, Kunming Metallurgy College, Kunming 650300, China; yunnanyejin@126.com (H.Z.); kiki158961326@163.com (Q.N.)
[3] School of Land Resources Engineering, Kunming University of Science and Technology, Kunming 650093, China; 20232201243@stu.kust.edu.cn
* Correspondence: yinshubiao@kust.edu.cn (S.Y.); lmx816@126.com (M.L.)

Abstract: This study employs microwave roasting to decompose smithsonite mineral (zinc carbonate) into zinc oxide, which then reacts with pyrite to sulfurize its surface, forming zinc sulfide. This process is beneficial for the flotation recovery of zinc oxide minerals. The surface sulfidation behavior of smithsonite under low-temperature microwave roasting conditions is examined through X-ray diffraction (XRD), X-ray photoelectron spectroscopy (XPS), scanning electron microscopy (SEM), and thermodynamic calculations. XRD and thermodynamic analysis indicate that smithsonite completely decomposes into zinc oxide at 400 °C. Introducing a small amount of pyrite as a sulfidizing reagent leads to the formation of sulfides on the surface of decomposed smithsonite. XPS analysis confirms that the sulfide formed on the surface is zinc sulfide. SEM analysis reveals that sulfides are distributed on the surface of smithsonite, and the average sulfur concentration increases with the pyrite dosage. Microwave-assisted sulfurization of smithsonite ($ZnCO_3$) was found to significantly enhance its floatability compared to conventional sulfurization methods. The optimal mass ratio of $ZnCO_3$ to FeS_2 is approximately 1:1.5, with the best temperature being 400 °C. These findings provide a technical solution for the application of microwave roasting in the efficient recovery of smithsonite through flotation.

Keywords: microwave roasting; sulfidation behavior; smithsonite; zinc sulfide

Citation: Kang, J.; Yin, S.; Li, M.; Zhang, X.; Wen, X.; Zhang, H.; Nie, Q.; Lei, T. Sulfidation of Smithsonite via Microwave Roasting under Low-Temperature Conditions. *Minerals* **2024**, *14*, 855. https://doi.org/10.3390/min14090855

Academic Editor: Przemyslaw B. Kowalczuk

Received: 4 July 2024
Revised: 16 August 2024
Accepted: 22 August 2024
Published: 23 August 2024

1. Introduction

Zinc is an important non-ferrous metal widely employed across electrical, mechanical, military, metallurgical, chemical, and pharmaceutical domains, and it plays a pivotal role in national economic development [1]. The majority of zinc metal is derived from zinc sulfide ores, with only a minor fraction sourced from zinc oxide ores. As industrial technology progresses, the demand for zinc metal products continues to grow, while the reservoirs of zinc sulfide ores are increasingly depleting, posing challenges in meeting the increasing demand [2]. Consequently, there is a pressing need to intensify the exploration and utilization of zinc oxide mineral resources [3]. China has abundant zinc mineral reserves, primarily concentrated in Yunnan, Sichuan, and other regions [4]. Various zinc oxide minerals exist, including smithsonite ($ZnCO_3$), hemimorphite ($Zn_4[Si_2O_7](OH)_2$) and willemite (Zn_2SiO_4). Among these, smithsonite is the most abundant and economically significant, rendering it the primary mineral in zinc oxide ores.

Smithsonite is generally recovered through two flotation methods. The first method involves direct flotation with fatty acid collectors, chelating agents, and amphoteric collectors, which is effective but costly. The second method involves pretreatment to form a sulfide

film on the mineral surface, followed by flotation with xanthate or dodecylamine collectors. While this method performs well and is widely used, it has lower selectivity [5]. From both application and economic perspectives, pre-sulfidization is more practical and cost-effective. Thus, enhancing the degree of sulfidization during the pre-sulfidization of smithsonite remains a critical issue [6–8]. Current sulfurization techniques are broadly categorized into surface sulfurization, mechanical sulfurization, hydrothermal sulfurization, sulfurization roasting, and others [9]. Surface sulfurization [10] entails adding a sulfidizing reagent to the ore pulp, which hydrolyzes and dissociates in the solution and then adsorbs onto the mineral surface and reacts to form ZnS. Mechanical sulfurization [11] involves altering the crystal structure of the mineral through mechanical force, inducing lattice distortion, and significantly enhancing the diffusion of sulfur elements within the mineral. Hydrothermal sulfurization [12] refers to thiosulfate flotation under high-pressure hot water conditions. In this process, elemental sulfur undergoes a disproportionation reaction, generating a large number of S^{2-} ions and a small number of SO_4^{2-} ions. These ions react with the valuable metal oxides in the smithsonite, converting the mineral particle surface and even the entire particle interior into sulfides. Sulfurization roasting involves converting metal oxides in refractory materials into sulfides through the addition of sulfidizing reagents or sulfur sources at a certain temperature under an inert or reducing atmosphere. For decades, sulfidation processes have been employed in the recovery of smithsonite.

Microwaves are electromagnetic waves with frequencies ranging from 300 MHz to 300 GHz, corresponding to wavelengths of approximately 1 m to 1 mm. Microwaves possess several unique characteristics, including penetrability, selective heating, low thermal inertia, phototaxis, information transmission, and non-ionization [13]. Compared with traditional heating methods, microwave heating offers selective heating, rapid heating speed, high efficiency, low energy consumption, and no pollution [14]. Therefore, microwaves can be utilized in various industrial processes. In mineral processing, microwaves are commonly used in the pre-treatment of minerals. Chen et al. [15] studied the thermal decomposition and dissociation behavior of manganese ore using microwave heating. The mineral was heated to 1000 °C in a short period, resulting in an increase in manganese content to 40%. M. W. Goldbaum et al. [16] demonstrated that microwaves can rapidly increase the temperature to 1100 °C within a few minutes. However, this rapid heating rate can lead to uneven heating of the object. Therefore, controlling the heating rate is a critical area of research. Additionally, microwave pre-treatment has shown promising results for ores such as copper carbonate, kyanite, lead–zinc, and ilmenite [17].

Due to the fact that current sulfidation roasting typically uses conventional roasting, research on the sulfidation of smithsonite under microwave fields is limited [18]. We propose a novel approach involving pyrite decomposition at lower temperatures in a microwave field, allowing for the resulting sulfur gas to adhere to the surface of smithsonite for sulfidation. During roasting, smithsonite also decomposes to form zinc oxide [19], making it more susceptible to sulfidation. This sulfurized smithsonite can then be more easily recovered by flotation. Consequently, this study aims to leverage microwave characteristics to sulfurize smithsonite ($ZnCO_3$) at a lower temperature using pyrite as a sulfidizing reagent and to investigate the sulfidation behavior. Characterizations are conducted through several techniques, including X-ray diffraction (XRD), X-ray photoelectron spectroscopy (XPS), and field-emission scanning electron microscopy (SEM), while the floatability of it is verified by flotation experiments.

2. Experimental

2.1. Experimental Materials

Both smithsonite and the sulfidizing reagent FeS_2 were purchased from Lanping, Yunnan, China. Figure 1 depicts the XRD patterns of the samples. The XRD patterns of the samples featured only smithsonite and pyrite, indicating high mineral purity. The smithsonite and pyrite were ground and crushed to a particle size range of 0.045–0.075 mm. Then, they were subjected to sieving and drying before being used for the experiment.

Flotation experiments employed butyl xanthate as a collector, pine oil as a frother, and copper sulfate ($CuSO_4$) as an activator. Sodium hydroxide (NaOH) was used to adjust the pulp pH, and sodium sulfide served as the sulfidizing reagent.

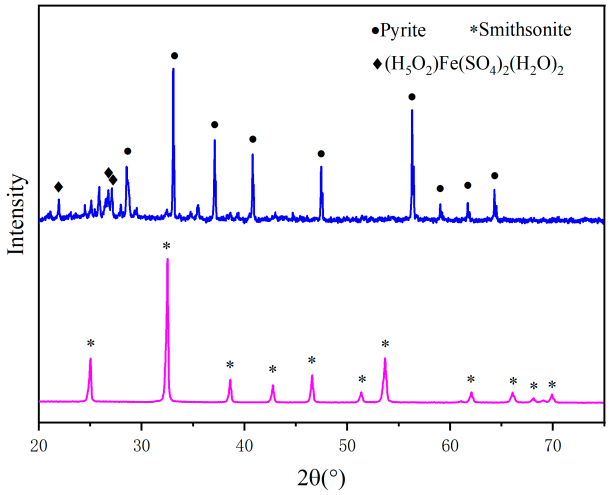

Figure 1. XRD pattern of the prepared samples.

2.2. Experimental Device and Operation Method

The experimental apparatus for the smithsonite sulfidation experiment included a microwave rotary tube furnace, a cooling water tank, and other supporting equipment. The experimental equipment diagram is shown in Figure 2.

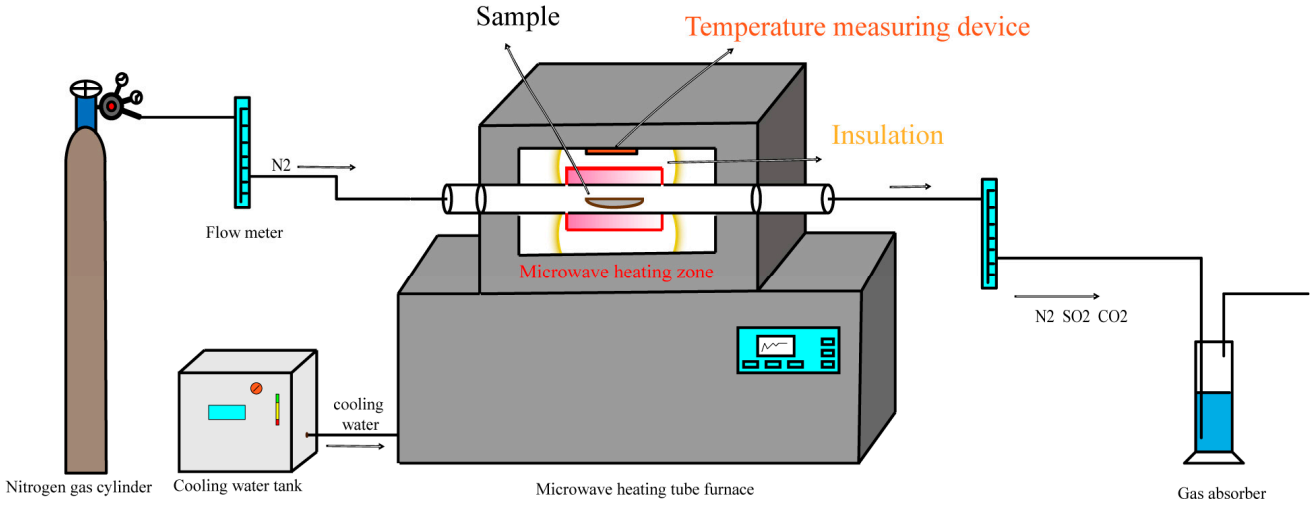

Figure 2. Microwave roasting experimental working system.

Typically, smithsonite and pyrite were blended in various mass ratios, ensuring even distribution by grinding in an agate mortar. The resulting mixture was then placed into a crucible boat, which was inserted into the tube furnace and evacuated before being purged with nitrogen. The microwave tube furnace was then activated, during which nitrogen flow was maintained until the cooling process. Once roasting was complete, the mixture was cooled to room temperature before removal. Subsequently, the composition was analyzed via XRD, XPS, and SEM techniques.

2.3. Characterization Method

The morphology of the samples under various mass ratios and temperatures was characterized using a field-emission scanning electron microscope (German ZEISS Sigma 300, Carl Zeiss AG, Oberkochen, Germany). Elemental distribution around the samples was analyzed via energy-dispersive X-ray spectroscopy. The detection was performed using a Rigaku Ultima IV X-ray powder diffractometer from Rigaku, Tokyo, Japan, with Cu Kα radiation (λ = 1.5406 Å). The chemical valence state of sulfur in the samples was analyzed via XPS (Thermo Scientific K-Alpha, Thermo Scientific, Waltham, MA, USA), with calibration fitting performed using Advantage v5.9921 software. Thermodynamics were simulated using HSC 6.0 software Reaction Equations to calculate the required Gibbs free energy for the reaction. Finally, graphing was conducted using Origin2018 software.

3. Results and Discussion

3.1. Thermodynamic Analysis

Thermodynamics plays a crucial role in the analysis of the roasting reaction. The thermodynamic properties of smithsonite sulfide roasting directly influence the quality of the process, and the analysis of the properties can offer a theoretical foundation. Hence, studying the standard Gibbs free energy of the reaction is vital. A literature search reveals potential reactions that may occur during smithsonite sulfurization roasting [20,21].

$$ZnCO_3 = ZnO + CO_2(g) \quad (1)$$

$$2FeS_2 = 2FeS + S_2(g) \quad (2)$$

$$4ZnO + 4SO_2(g) = ZnS + 3ZnSO_4 \quad (3)$$

$$4ZnO + 3S_2(g) = 4ZnS + 2SO_2(g) \quad (4)$$

$$14ZnO + 6FeS_2 = 3ZnFe_2O_4 + SO_2(g) + 11ZnS \quad (5)$$

Changes in standard Gibbs free energy during normal heating from 0 to 800 °C are calculated using the HSC 6.0 software, as illustrated in Figure 3.

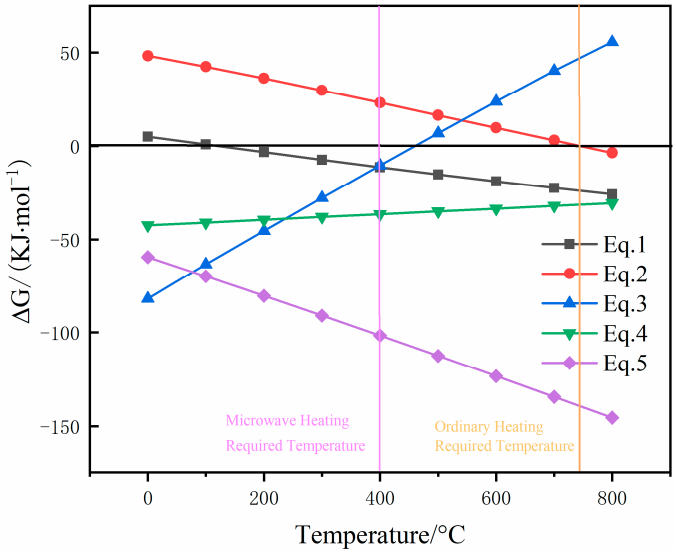

Figure 3. Gibbs free energy diagram at 800 °C.

As depicted in Figure 3, smithsonite initiates decomposition at temperatures below 400 °C (Equation (1)). Pyrite begins to decompose when the Gibbs free energy turns negative at approximately 750 °C (Equation (2)). However, according to the literature, under microwave conditions, pyrite starts to partially decompose at 400 °C and fully decomposes

into FeS at 500 °C–600 °C. Compared with conventional methods, microwave heating reduces the necessary temperature by approximately 100 °C. Different from traditional heating, microwave heating converts energy directly into internal heat through molecular interactions, allowing for pyrite to rapidly reach its decomposition temperature. Moreover, the microwave heating process creates a porous structure in pyrite, which facilitates the release of decomposed sulfur gases and promotes further reactions [22–24]. Among the three sulfidation equations (Equations (3)–(5)), at 400 °C, the reaction between zinc oxide and pyrite exhibits a more negative Gibbs free energy than the other two reactions, facilitating the transformation of ZnO into ZnS. The change in Gibbs free energy of the reaction equations indicates the thermodynamic feasibility of smithsonite sulfidation roasting under standard conditions. According to the reaction equations, pyrite decomposes into sulfur and iron sulfide (Equation (2)). Subsequently, the ZnO resulting from smithsonite decomposition (Equation (1)) undergoes sulfidation (Equation (4)). Additionally, pyrite can directly interact with ZnO to yield zinc ferrite, sulfur dioxide, and zinc sulfide (Equation (5)). Furthermore, ZnO can react with the generated sulfur dioxide gas to form zinc sulfide and zinc sulfate (Equation (3)).

3.2. XRD Analysis

First, we investigated the decomposition temperature of smithsonite under microwave roasting. The analysis of the raw smithsonite is shown in Figure 1 and its states after roasting at two different temperatures (Figure 4a,b) revealed that smithsonite completely decomposed at 400 °C. The decomposition product, zinc oxide, then participated in subsequent sulfidation reactions. Figure 5 illustrates the roasting product of pyrite at 400 °C, indicating that some pyrite had started to decompose. This early onset of decomposition, where decomposition typically starts around 750 °C (Figure 3), offers a significant advantage. This advantage stems from pyrite's exceptional microwave-absorbing properties [25]; within the microwave field, pyrite absorbs microwaves, and the stored energy is directly converted into heat through molecular interactions, thereby altering the phase transition temperature of pyrite.

To further investigate the influence of different conditions on sulfidation, we conducted XRD analysis on products subjected to varying roasting temperatures and mass ratios. The XRD patterns at different temperatures are depicted in Figure 6a–c. The characteristic peaks of smithsonite exist at 350 °C but disappear at 400 °C and 450 °C, thereby confirming the accuracy of smithsonite decomposition temperature. Additionally, the emergence of zinc sulfide characteristic peaks indicates a reaction between the decomposition products of smithsonite and pyrite, leading to the formation of zinc sulfide and the completion of the sulfidation reaction. However, under the 450 °C roasting condition, a significant amount of zinc ferrite ($ZnFe_2O_4$) is generated, and the intensity of the zinc sulfide peaks decreases, thus establishing the optimal temperature as 400 °C. In Figure 7a–c, alongside the characteristic peaks of zinc sulfide, the presence of zinc ferrite peaks also supports the validity of Equation (5). A comparison of Figure 7b with Figure 7a,c reveals that the characteristic peaks of zinc sulfide and iron zinc in Figure 7b are higher than those of the other two mass ratios. Additionally, the intensity of the pyrite characteristic peak in Figure 7b is similar to that in Figure 7a but lower than that in Figure 7c. These observations suggest incomplete reactions when pyrite is present in low proportions, resulting in partial reaction with smithsonite. Conversely, in the presence of a higher pyrite content, the reaction with smithsonite is more thorough, leading to the increased crystallization of zinc sulfide. However, when the mass ratio reaches a certain level, partially decomposed pyrite reacts with all the smithsonite, leaving an excess of undecomposed pyrite. This excess results in an increased pyrite characteristic peak and a reduction in the peaks of zinc sulfide and zinc ferrite.

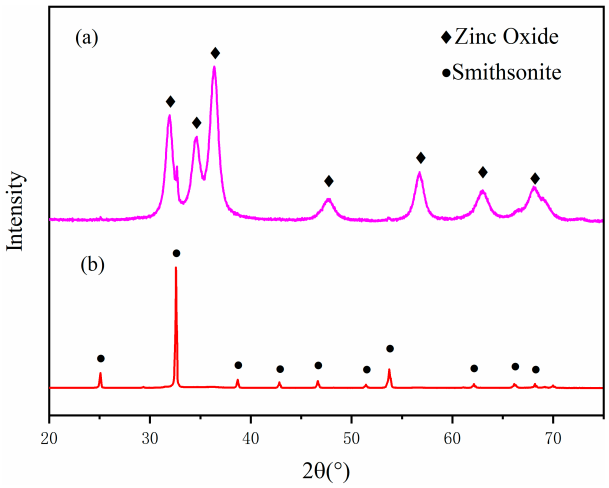

Figure 4. Comparison of XRD patterns of smithsonite under different microwave temperatures: (**a**) 400 °C; (**b**) 300 °C.

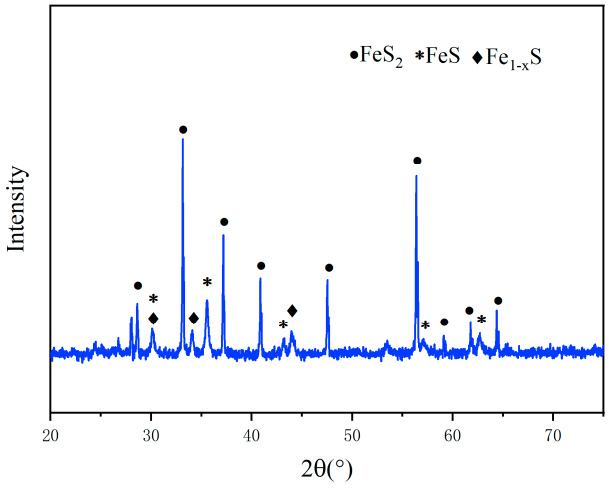

Figure 5. XRD pattern of pyrite at 400 °C under microwave roasting.

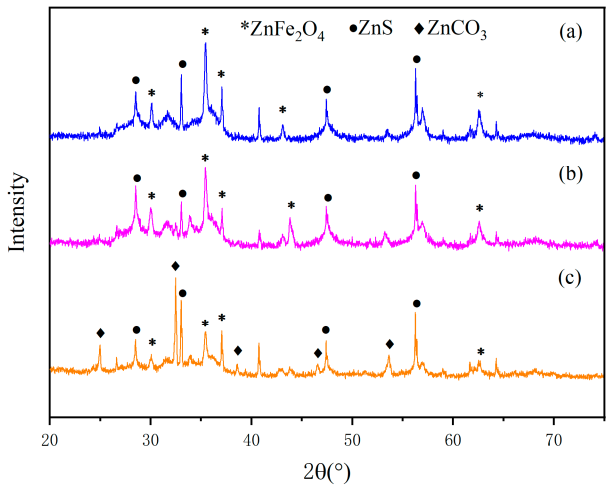

Figure 6. Comparison of the XRD patterns of smithsonite and pyrite under different calcination temperature conditions: (**a**) 450 °C; (**b**) 400 °C; (**c**) 350 °C.

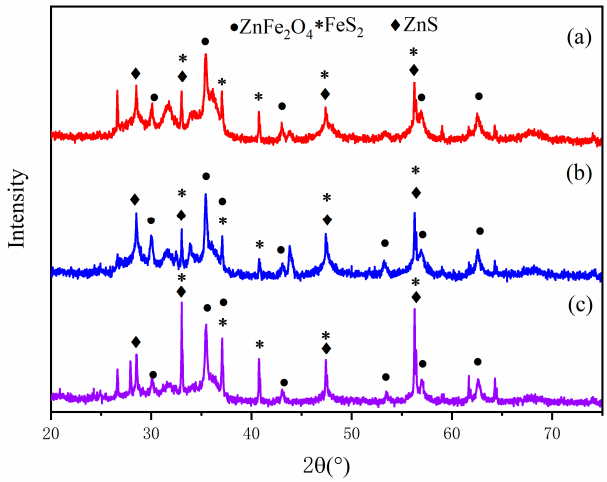

Figure 7. Comparison of the XRD patterns smithsonite and pyrite under different $ZnCO_3$:FeS_2 mass ratios conditions: (**a**) 1:1; (**b**) 1:1.5; (**c**) 1:2.

3.3. Sulfidation Surface Analysis

Figure 8a illustrates the S2p spectrum of smithsonite. The S2 peak is fitted with four components. The binding energies at 161.76 eV for sample A, 161.43 eV for sample B, and 161.93 eV for sample C correspond to S in the formed zinc sulfide [26]. Another set of binding energies at 162.86 eV for sample A, 162.52 eV for sample B, and 163.03 eV for sample C correspond to S_2^{2-} in the formed iron sulfides [27]. Peaks at 168.62 eV and 169.72 eV for sample A, 168.21 eV and 169.31 eV for sample B, and 168.88 eV and 169.9 eV for sample C correspond to SO_4^{2-} [28] from the reactions producing zinc oxide (Equation (3)) and the sulfate iron contained in some pyrite. The relative contents of S2p in the three groups of samples are shown in Table 1. As depicted in Table 1, as the FeS_2 dosage gradually increases, the percentage of S in ZnS on the mineral surface decreases, while the percentage of S in SO_4^{2-} increases. Additionally, the ratio between iron sulfides and zinc sulfides also increases with the increase in the mass ratio, consistent with the XRD analysis. Therefore, combined with the XRD analysis, the optimal ratio is determined as 1:1.5.

The C1s spectrum of smithsonite is shown in Figure 8b. The C1 peak was deconvoluted into three components. The binding energies for samples A, B, and C show peaks near 284.81 eV and 288.55 eV, with 284.81 eV serving as the reference peak and 288.55 eV corresponding to carbonate. The peak at 286.52 eV represents carbonyl carbon (C=O) [29], indicating that a small amount of zinc carbonate remains undecomposed after microwave roasting at 400 °C. This finding is consistent with the observation in Table 2, where the content of zinc carbonate decreases as the mass ratio increases. We believe that there are two reasons for the presence of undecomposed smithsonite. First, uneven microwave heating may contribute to incomplete decomposition. Second, during the mixing process, pyrite may encapsulate zinc carbonate, preventing some of the encapsulated zinc carbonate from fully decomposing when heated.

Figure 8c presents the O1s profile of smithsonite, and an analysis in conjunction with Table 3 reveals the presence of metal oxides and metal carbonates in the samples [30,31]. This supports the process by which zinc oxide forms from the decomposition of smithsonite. The table also shows that the percentage of zinc oxide is lower than the content of zinc carbonate. This discrepancy is attributed to the reaction of zinc oxide with sulfur, which reduces the proportion of zinc oxide. As the mass ratio increases, the zinc oxide content decreases. However, under a 1:2 mass ratio, the percentage of zinc oxide increases. This increase indicates that, at a 1:1.5 ratio, the reaction between zinc oxide and pyrite reaches its limit, leading to a higher zinc oxide content at the 1:2 ratio. Therefore, based on Figure 8 and the XRD analysis, the optimum mass ratio of 1:1.5 was determined.

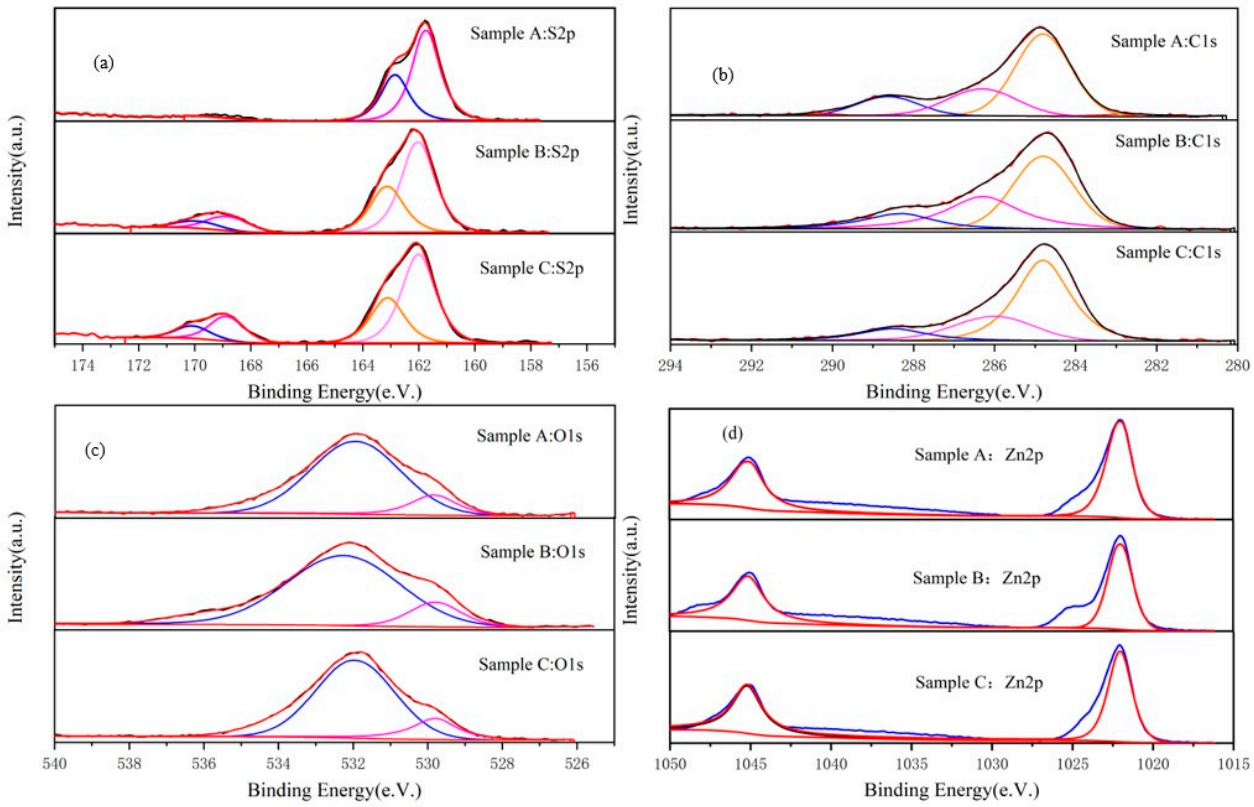

Figure 8. XPS spectra of samples with different mass ratios of $ZnCO_3$:FeS_2: 1:1 (sample A), 1:1.5 (sample B), and 1:2 (sample C); (**a**) S2p spectrum of smithsonite; (**b**) C1s spectrum of smithsonite; (**c**) O1s profile of smithsonite; (**d**) Zn2p spectra for samples with different $ZnCO_3$/FeS_2 mass ratios.

Table 1. Binding energy and relative content of S2p in different samples.

$ZnCO_3/FeS_2$ Mass Ratio	Binding Energy (eV)				Relative Contents (%)		
	$FeSO_4$	$ZnSO_4$	Iron Sulfides	ZnS	$Fe/ZnSO_4$	Iron Sulfides	ZnS
1:1	168.62	169.72	162.86	161.76	4.32	38.78	38.72
1:1.5	168.21	169.31	162.53	161.43	14.9	42.62	42.71
1:2	168.88	169.98	163.03	161.93	22.53	47.82	47.86

Table 2. Binding energy and relative content of C1s in different samples.

$ZnCO_3/FeS_2$ Mass Ratio	Binding Energy (eV)		Relative Contents (%)	
	C	CO_3^{2-} C-O-C	$ZnCO_3$	C
1:1	284.82	288.74 286.34	24.35	75.65
1:1.5	284.79	288.43 286.38	23.73	76.22
1:2	284.77	288.59 286.12	15.79	84.21

Table 3. Binding energy and relative content of O1s in different samples.

$ZnCO_3/FeS_2$ Mass Ratio	Binding Energy (eV)		Relative Contents (%)	
	Metal Oxide	Metal Carbonates	ZnO	$ZnCO_3$
1:1	529.71	531.93	11.05	88.95
1:1.5	529.14	532.27	10.27	89.73
1:2	529.77	531.96	10.44	89.56

Figure 8d shows the Zn2p spectra for samples with different $ZnCO_3/FeS_2$ mass ratios. The $Zn2p_{3/2}$ spectra exhibit high symmetry around 1022.06 eV, making it difficult to distinguish between ZnS and ZnO species, as their Zn atomic binding energies are close to 1022.00 eV. Nevertheless, the presence of ZnS has been confirmed based on the variation in S atomic concentration on the sample surface, as shown in Figure 8a and Table 1.

The surface morphology and elemental composition of the pyrite/smithsonite particles after microwave roasting were analyzed through SEM–EDS. Figure 9 shows the morphology of the pyrite/smithsonite samples treated at 300 °C. The SEM micrographs of Figure 9a,b show that the surface of the sample treated with microwave heat treatment at 300 °C is relatively smooth and dense, with clear edges and corners. Figure 9c shows the SEM map of a single element, revealing that sulfur is overlaid on zinc, indicating that sulfur is enriched on the smithsonite. The EDS spectrum in Figure 9d shows that the concentration of zinc atoms on the mineral surface is higher than that of sulfur atoms, and the carbon content is also elevated. This suggests that, at this temperature, the decomposition of smithsonite and pyrite is minimal, resulting in a low degree of sulfidation. Figures 10 and 11 display the morphology of samples treated at 400 °C with two different mass ratios of 1:1.5 and 1:2. Figures 10 and 11 include SEM images (a), (b), and (c), with (c) showing the spectrum for a single element, while (d) represents the EDS spectrum. The point-scanning EDS spectrum is labeled as 1, 2. The sample surface becomes loose and porous, and a large number of particles are attached to the surface. Point scanning and area scanning of the mineral surface reveal that the fine particles on the surface are pyrite. Analysis of both area scanning and point scanning results reveals a reduction in the zinc content proportion on the surface, indicating the decomposition of pyrite. Sulfur gas reacts with the zinc oxide produced through the decomposition of smithsonite on the mineral surface. Additionally, undecomposed pyrite interacts with the smithsonite on the surface, resulting in the formation of a sulfide layer on the mineral surface. A comparison of the results of Figures 10 and 11 reveals that both groups of samples heated at 400 °C in the microwave exhibit a significant amount of sulfur adhering to the mineral surface. Furthermore, as the pyrite dosage increases, the sulfur-to-zinc content ratio on the mineral surface correspondingly increases. However, EDS spectroscopy analysis indicates minimal variation in sulfur element content under the mass ratio conditions of 1:1.5 and 1:2. The analysis above indicates that the temperature rise facilitates the decomposition of FeS_2 and $ZnCO_3$. The decomposition of smithsonite renders the surface loose and porous, facilitating the accumulation of sulfur on the smithsonite surface, thereby exerting a sulfidation effect on smithsonite. Additionally, once a particular mass ratio is attained, the sulfur saturation point on the surface of smithsonite is reached, as the mineral surface can only accommodate a certain amount of sulfur and cannot bind more. Given the similarity in results between the two ratios at 400 °C, we select the 1:1.5 mass ratio as the optimal configuration.

3.4. Flotation Experiment Verification

To evaluate the practical applicability of microwave-assisted sulfurization, flotation comparison tests were conducted using a XFGII micro-flotation machine (effective cell volume: 40 mL). Ten grams of raw smithsonite and ten grams of microwave-roasted sample (with a 1:1.5 smithsonite-to-pyrite mass ratio) were subjected to flotation experiments. Flotation reagents were added sequentially and left to react for a predetermined duration. The flotation test procedures are illustrated in Figure 12a,b.

The flotation behavior of smithsonite was investigated using two distinct methods: conventional sulfurization and microwave-assisted sulfurization. Figure 12a illustrates the conventional sulfurization process, commencing with the addition of sodium sulfide to promote the sulfurization of the smithsonite. This was followed by sequential additions of copper sulfate (activation), butyl xanthate (collector), and pine oil (frother). Froth flotation was then conducted for three minutes, yielding concentrate 1 and tailings 1. Optimization studies revealed that the optimal reagent dosages for conventional sulfurization flotation

were 300 g/t sodium sulfide, 60 g/t copper sulfate, 50 g/t butyl xanthate, and 10 g/t pine oil.

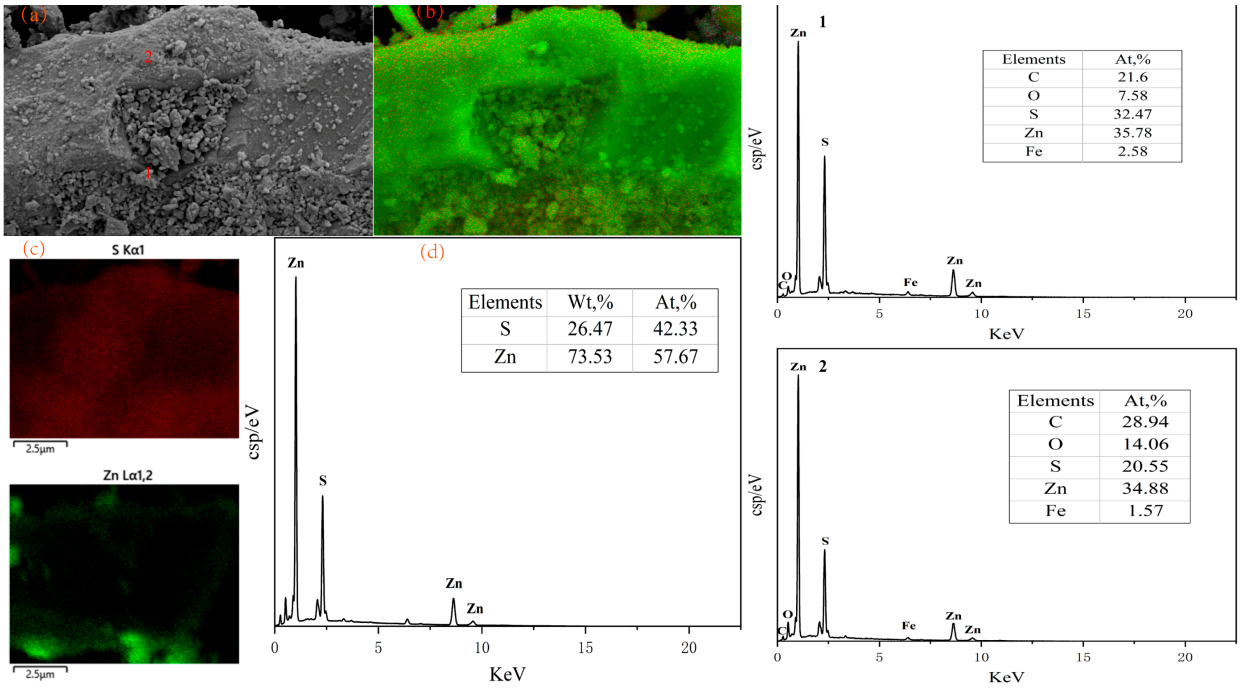

Figure 9. SEM–EDS spectra of the $ZnCO_3$:FeS_2 sample after treatment at 300 °C: (**a**,**b**) the morphology of the pyrite/smithsonite samples treated at 300 °C; (**c**) SEM map of a single element, revealing that sulfur is overlaid on zinc, indicating that sulfur is enriched on the smithsonite; (**d**) EDS spectrum of the ZnCO3:FeS2 sample after treatment at 300 °C. The point-scanning EDS spectrum is labeled as 1, 2.

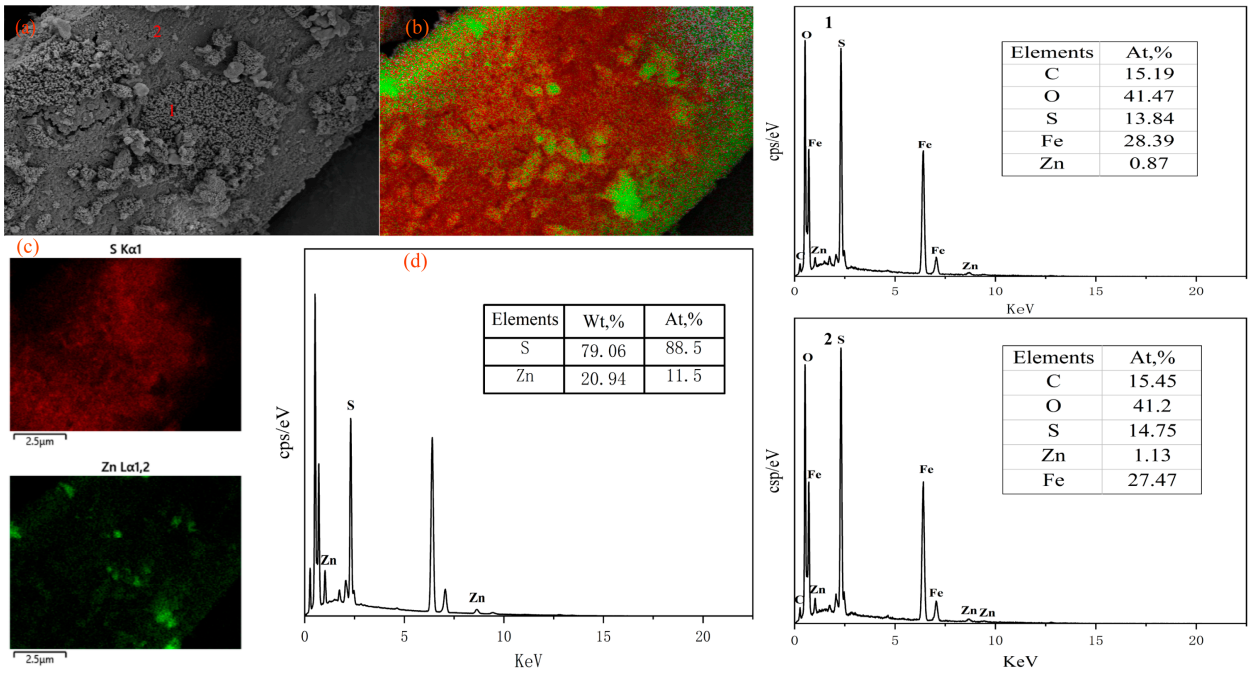

Figure 10. SEM–EDS spectra of the sample with a $ZnCO_3$:FeS_2 mass ratio of 1:1.5 after treatment at 400 °C: (**a**,**b**) SEM images; (**c**) SEM map of a single element; (**d**) EDS spectrum. The point-scanning EDS spectrum is labeled as 1, 2.

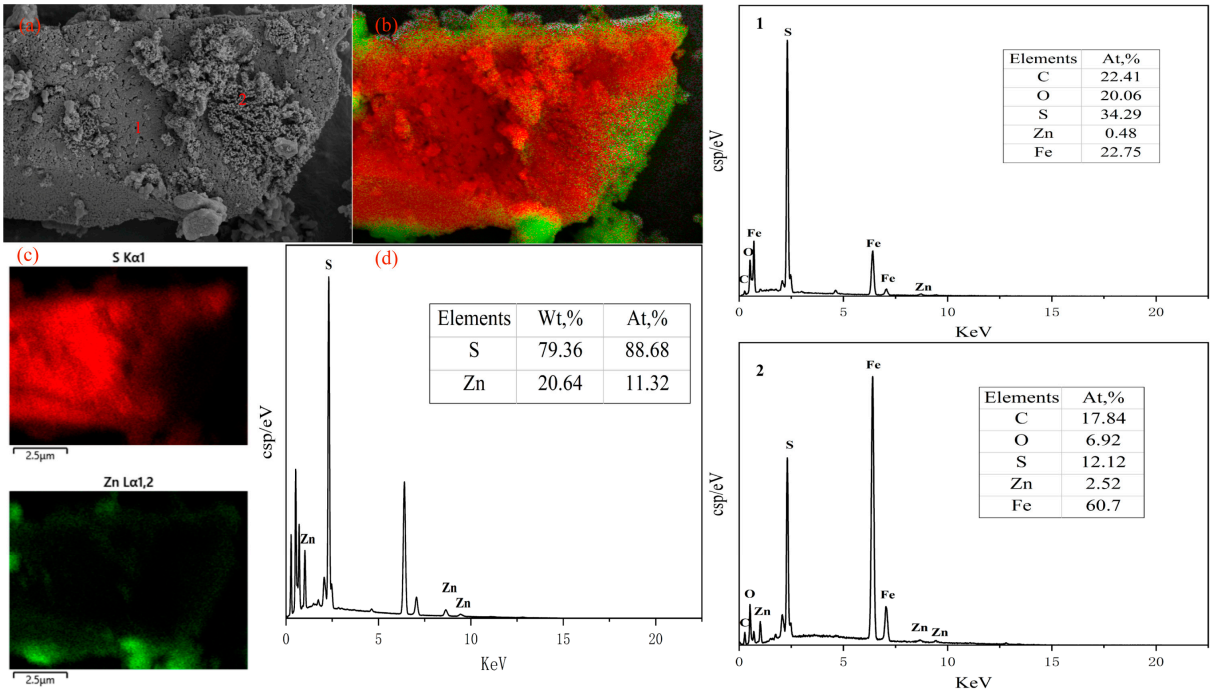

Figure 11. SEM–EDS spectrum of the sample with a $ZnCO_3$:FeS_2 mass ratio of 1:2 after treatment at 400 °C: (**a**,**b**) SEM images; (**c**) SEM map of a single element; (**d**) EDS spectrum. The point-scanning EDS spectrum is labeled as 1, 2.

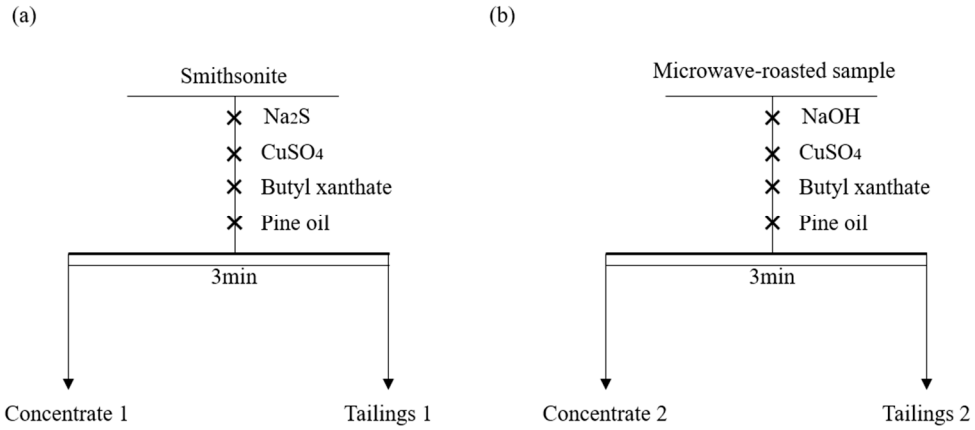

Figure 12. Flowchart of flotation process with different sulfidation methods: (**a**) the conventional sulfurization process, (**b**) flotation procedure for the microwave-roasted sample.

Figure 12b depicts the flotation procedure for the microwave-roasted sample. In this method, sodium hydroxide was initially added to adjust the pH to 11.5, suppressing the flotation of pyrite. Subsequently, copper sulfate (60 g/t), butyl xanthate (50 g/t), and pine oil (10 g/t) were added in sequence. After a 3-min flotation period, the resulting slurry was filtered and dried to obtain concentrate 2 and tailings 2. The final flotation results, including grade analysis and recovery rate, are summarized in Tables 4 and 5, respectively.

Table 4. Experimental results of conventional flotation of smithsonite.

Product Name	Yield/%	Grade/%	Recovery Rate/%
Concentrate 1	71.70	48.56	71.70
Tailings 1	28.30	48.56	28.30
Smithsonite	100.00	48.56	100.00

Table 5. Microwave-roasted smithsonite flotation experiment.

Product Name	Yield/%	Grade/%	Recovery Rate/%
Concentrate 2	34.93	50.21	90.32
Tailings 2	65.07	2.89	9.68
Microwave-roasted sample	100.00	19.42	100.00

A comparison of the flotation results presented in Tables 4 and 5 reveals a lower concentrate yield for the microwave-roasted sample compared to conventional sulfurization. This disparity stems from the inherent difference in sample composition. The 10 g sample used for microwave roasting comprised a 1:1.5 mixture of smithsonite and pyrite, with only 4 g of smithsonite present. Conversely, the smithsonite sample used in the conventional sulfurization process weighed 10 g, leading to a higher concentrate yield for concentrate 1. Despite the lower initial smithsonite content, microwave-assisted sulfurization followed by flotation yielded a zinc concentrate with a grade of 50.21% and a recovery rate of 90.32%. This represents a 1.65% increase in zinc grade and a significant 18.62% improvement in recovery rate compared to the conventional sulfurization method. These findings highlight the superior sulfurization efficiency achieved through microwave roasting. While microwave roasting sulfurization incurs slightly higher production costs due to energy consumption, the enhanced flotation indicators and improved zinc recovery demonstrate its potential as a viable alternative to conventional methods. This novel approach offers a promising technical solution for the effective recovery and utilization of challenging oxidized zinc ores.

4. Conclusions

The effects of microwave roasting on the micro-morphology and sulfur transformation during the sulfidation process of smithsonite under various conditions were investigated through comparative studies. The sulfidized minerals were characterized through XRD, XPS, and SEM–EDS analyses. The effectiveness of microwave roasting for enhancing the flotation recovery of smithsonite was investigated through comparative flotation experiments with the conventionally sulfidized method. According to the results, the following conclusions can be obtained:

1. Thermodynamic analysis indicates that the sulfidation of zinc carbonate is thermodynamically feasible, with an increase in temperature favoring ZnS formation.
2. According to the analysis by XRD and XPS, when the pyrite content is low, the crystallinity degree of the generated sulfidized zinc is low. Conversely, when pyrite is in excess, most of the smithsonite completely reacts, leaving behind a large amount of pyrite. Additionally, as the FeS_2 dosage increases, the proportions of zinc sulfate and iron sulfate also increase.
3. SEM–EDS analysis reveals that the smithsonite surface appears relatively smooth and flat at 300 °C. However, when the temperature reaches 400 °C, the mineral surface becomes loose and porous, owing to the occurrence of gas pores generated by the decomposition of smithsonite into CO_2. With the increase in the FeS_2 dosage, the concentration of sulfur atoms on the smithsonite surface gradually increases. However, once a certain mass ratio is reached, the concentration of sulfur elements on the mineral surface remains roughly unchanged, indicating that the theoretical mass ratio for the complete conversion of smithsonite to zinc sulfide has been achieved.
4. According to the results of the three analytical methods, the optimal microwave roasting conditions are determined as follows: a microwave roasting temperature of 400 °C and a $ZnCO_3$:FeS_2 mass ratio of 1:1.5.
5. Comparative flotation experiments demonstrated that microwave-roasted smithsonite exhibited significantly higher floatability than the conventionally sulfidized method.

Author Contributions: Conceptualization, H.Z.; Methodology, M.L. and H.Z.; Software, J.K.; Validation, J.K., X.Z. and X.W.; Data curation, J.K.; Writing—original draft, J.K.; Writing—review & editing, S.Y. and M.L.; Supervision, S.Y., M.L. and T.L.; Project administration, M.L., H.Z. and Q.N.; Funding acquisition, M.L. All authors have read and agreed to the published version of the manuscript.

Funding: This work was supported by the Young Talent Special Project of Yunnan Province's Xingdian Elite Support Program (No. YNWR-QNBJ-2019-086), the General Project of Yunnan Provincial Basic Research Program (No. 202201AT070069), and the Doctoral Research Startup Fund Project of Kunming Metallurgy College (No. Xxrcxm202101).

Data Availability Statement: The original contributions presented in the study are included in the article, further inquiries can be directed to the corresponding author.

Acknowledgments: The authors gratefully acknowledge the comments from three anonymous reviewers and the academic editors for their constructive reviews of the manuscript.

Conflicts of Interest: The authors declare no conflicts of interest.

References

1. Cai, J.; Liu, D.; Shen, P.; Zhang, X.; Song, K.; Jia, X.; Su, C. Effects of Heating-Sulfidation on the Formation of Zinc Sulfide Species on Smithsonite Surfaces and Its Response to Flotation. *Min. Eng.* **2021**, *169*, 106956. [CrossRef]
2. Liao, R.; Wen, S.; Liu, J.; Bai, S.; Feng, Q. Synergetic Adsorption of Dodecylamine and Octyl Hydroxamic Acid on Sulfidized Smithsonite: Insights from Experiments and Molecular Dynamics Simulation. *Sep. Purif. Technol.* **2024**, *329*, 125106. [CrossRef]
3. Feng, Q.; Zhao, G.; Zhang, G.; Zhao, W.; Han, G. Degradation Mechanism of Surface Hydrophobicity by Ferrous Ions in the Sulfidization Flotation System of Smithsonite. *Colloids Surf. A Physicochem. Eng. Asp.* **2022**, *648*, 129119. [CrossRef]
4. Lv, J.; Tong, X.; Zheng, Y.; Xie, X.; Wang, C. Study on the Surface Sulfidization Behavior of Smithsonite at High Temperature. *Appl. Surf. Sci.* **2018**, *437*, 13–18. [CrossRef]
5. Chen, H.; Xie, H.; Chen, J.; Jin, Y.; Zeng, P.; Song, Z.; Zhang, Q.; Liu, D. Research Progress on Flotation Collectors for Lead-Zinc Oxide Ore. *Conserv. Util. Miner. Resour.* **2023**, *43*, 42–53. [CrossRef]
6. Li, Y.; Wang, J.; Wei, C.; Liu, C.-X.; Jiang, J.-B.; Wang, F. Sulfidation Roasting of Low Grade Lead–Zinc Oxide Ore with Elemental Sulfur. *Min. Eng.* **2010**, *23*, 563–566. [CrossRef]
7. Zhou, H.; Guo, J.; Zhu, G.; Xu, H.; Tang, X.; Luo, X. Flotation Behavior and Mechanism of Smithsonite under the System of Bidentate Ligand Sulfide Sodium Thiocyanate. *Sep. Purif. Technol.* **2024**, *334*, 126086. [CrossRef]
8. Zheng, H.; Zhang, G.; Li, C.; Li, B.; Ye, G. The Surface Dissolution Process of Smithsonite and Its Effect on Flotation Behaviour. *Colloids Surf. A Physicochem. Eng. Asp.* **2023**, *676*, 132118. [CrossRef]
9. Han, J.; Liu, W.; Zhang, T.; Xue, K.; Li, W.; Jiao, F.; Qin, W. Mechanism Study on the Sulfidation of ZnO with Sulfur and Iron Oxide at High Temperature. *Sci. Rep.* **2017**, *7*, 42536. [CrossRef]
10. Feng, Q.; Wen, S. Formation of Zinc Sulfide Species on Smithsonite Surfaces and Its Response to Flotation Performance. *J. Alloys Compd.* **2017**, *709*, 602–608. [CrossRef]
11. Yin, Z.; Cagnetta, G.; Huang, J. Mechanochemically Sulfidated Zero-Valent Iron as Persulfate Activation Catalyst in Permeable Reactive Barriers for Groundwater Remediation—A Feasibility Study. *Chemosphere* **2023**, *311*, 137081. [CrossRef] [PubMed]
12. Ke, Y.; Min, X.-B.; Chai, L.-Y.; Zhou, B.-S.; Xue, K. Sulfidation Behavior of Zn and ZnS Crystal Growth Kinetics for $Zn(OH)_2$–S–NaOH Hydrothermal System. *Hydrometallurgy* **2016**, *161*, 166–173. [CrossRef]
13. Zheng, X.; Chen, G.; Chen, J.; Peng, J.; Srinivasakannan, C.; Ruan, R. Preparation of Synthetic Rutile from High Titanium Slag Using Microwave Heating. *Phase Transit.* **2018**, *91*, 308–315. [CrossRef]
14. Chen, G.; Ling, Y.; Li, Q.; Zheng, H.; Qi, J.; Li, K.; Chen, J.; Peng, J.; Gao, L.; Omran, M.; et al. Investigation on Microwave Carbothermal Reduction Behavior of Low-Grade Pyrolusite. *J. Mater. Res. Technol.* **2020**, *9*, 7862–7869. [CrossRef]
15. Li, K.; Chen, J.; Peng, J.; Ruan, R.; Srinivasakannan, C.; Chen, G. Pilot-Scale Study on Enhanced Carbothermal Reduction of Low-Grade Pyrolusite Using Microwave Heating. *Powder Technol.* **2020**, *360*, 846–854. [CrossRef]
16. Goldbaum, M.W.; Elliott, R.; Forster, J.; Maham, Y.; Bobicki, E.R. Investigating the Microwave Heating Behaviour of Pyrrhotite Tailings. *Min. Eng.* **2020**, *146*, 106152. [CrossRef]
17. Huang, W.; Liu, Y. Study on Microwave-Assisted Grinding and Liberation Characteristics for Ludwigite. *J. Microw. Power Electromagn. Energy* **2021**, *55*, 28–44. [CrossRef]
18. Chen, Y.; Sun, Y.; Han, Y. Efficient Flotation Separation of Lead–Zinc Oxide Ores Using Mineral Sulfidation Reconstruction Technology: A Review. *Green. Smart Min. Eng.* **2024**, *1*, 175–189. [CrossRef]
19. Zhang, Y.; Deng, J.; Chen, J.; Yu, R.; Xing, X. A Low-Cost and Large-Scale Synthesis of Nano-Zinc Oxide from Smithsonite. *Inorg. Chem. Commun.* **2014**, *43*, 138–141. [CrossRef]
20. Lan, Z.; Lai, Z.; Zheng, Y.; Lv, J.; Pang, J.; Ning, J. Thermochemical Modification for the Surface of Smithsonite with Sulfur and Its Flotation Response. *Min. Eng.* **2020**, *150*, 106271. [CrossRef]
21. Zheng, Y.; Liu, W.; Qin, W.; Jiao, F.; Han, J.; Yang, K.; Luo, H. Sulfidation Roasting of Lead and Zinc Carbonate with Sulphur by Temperature Gradient Method. *J. Cent. South. Univ.* **2015**, *22*, 1635–1642. [CrossRef]

22. Zhang, X.; Kou, J.; Sun, C. A Comparative Study of the Thermal Decomposition of Pyrite under Microwave and Conventional Heating with Different Temperatures. *J. Anal. Appl. Pyrolysis* **2019**, *138*, 41–53. [CrossRef]
23. Tian, C.; Rao, Y.; Su, G.; Huang, T.; Xiang, C. The Thermal Decomposition Behavior of Pyrite-Pyrrhotite Mixtures in Nitrogen Atmosphere. *J. Chem.* **2022**, *2022*, 1–11. [CrossRef]
24. Liu, L.; Liu, Q.; Zhang, K.; Zhang, S.; Li, K.; Li, J.; Peng, G. Thermal Decomposition and Oxidation of Pyrite with Different Morphologies in the Coal Gangue of North China. *J. Therm. Anal. Calorim.* **2023**, *148*, 2023–2038. [CrossRef]
25. He, C.L.; Ma, S.J.; Su, X.J.; Mo, Q.H.; Yang, J.L. Comparison of the Microwave Absorption Characteristics of Hematite, Magnetite and Pyrite. *J. Microw. Power Electromagn. Energy* **2015**, *49*, 131–146. [CrossRef]
26. Liu, W.; Zhu, L.; Han, J.; Jiao, F.; Qin, W. Sulfidation Mechanism of ZnO Roasted with Pyrite. *Sci. Rep.* **2018**, *8*, 9516. [CrossRef]
27. Meng, Q.; Yuan, Z.; Du, Y.; Wang, J. Sulfuric Acid Pretreatment of Oxidized Pyrrhotite in Flotation Desulphurization of Magnetite Concentrate. *Min. Eng.* **2023**, *203*, 108347. [CrossRef]
28. Zheng, Y.; Bao, L.; Lv, J.; Pang, J.; Hu, P.; Huang, Y. Flotation Response of Cerussite after Hydrothermal Treatment with Sulfur and the Sulfidation Mechanism. *J. Mater. Res. Technol.* **2021**, *15*, 2933–2942. [CrossRef]
29. Li, C.; Bai, S.; Ding, Z.; Yu, P.; Wen, S. Visual MINTEQ Model, ToF–SIMS, and XPS Study of Smithsonite Surface Sulfidation Behavior: Zinc Sulfide Precipitation Adsorption. *J. Taiwan Inst. Chem. Eng.* **2019**, *96*, 53–62. [CrossRef]
30. Xu, L.; Liu, D.; Sun, R.; Wang, Y.; Liu, Z.; Shao, P.; Wang, C.; Wen, S. Flotation Separation of Smithsonite and Calcite in Sodium Oleate System Using Soluble Starch as Depressant. *Min. Eng.* **2024**, *205*, 108490. [CrossRef]
31. Duchoslav, J.; Steinberger, R.; Arndt, M.; Stifter, D. XPS Study of Zinc Hydroxide as a Potential Corrosion Product of Zinc: Rapid X-ray Induced Conversion into Zinc Oxide. *Corros. Sci.* **2014**, *82*, 356–361. [CrossRef]